



ELSEVIER

Available online at www.sciencedirect.com

SCIENCE @ DIRECT®

PHYSICS LETTERS A

Physics Letters A 320 (2003) 47–52

www.elsevier.com/locate/pla

Picture of the low-dimensional structure in chaotic dripping faucets

Ken Kiyono^{a,*}, Tomoo Katsuyama^b, Takuya Masunaga^c, Nobuko Fuchikami^c

^a Educational Physiology Laboratory, Graduate School of Education, University of Tokyo, 7-3-1 Hongo, Bunkyo, Tokyo 113-0033, Japan

^b Division of Liberal Arts, Numazu College of Technology, 3600 Ooka, Numazu 410-8501, Japan

^c Department of Physics, Tokyo Metropolitan University 1-1, Minami-Ohsawa, Hachioji, Tokyo 192-0397, Japan

Received 5 August 2003; received in revised form 20 October 2003; accepted 21 October 2003

Communicated by C.R. Doering

Abstract

Chaotic dynamics of the dripping faucet was investigated both experimentally and theoretically. We measured continuous change in the position and velocity of the center of mass of the pendant drop prior to its detachment using a high-speed camera. Continuous trajectories of a low-dimensional chaotic attractor were reconstructed from these data, which was not previously obtained but predicted in our fluid dynamic simulation. From the simulation, we further obtained an approximate potential function with only two variables, the mass of the pendant drop and the position of the center of mass. The potential landscape helps one to understand intuitively how the dripping dynamics can exhibit low-dimensional chaos.

© 2003 Elsevier B.V. All rights reserved.

PACS: 05.45.Ac

Keywords: Dripping faucet dynamics; Chaos; Strange attractor; Drop formation

The rhythm of a dripping water faucet is not always regular and sometimes exhibits irregular behavior, which sensitively depends on the flow rate. It is nowadays well known that the irregularity of this system arises from deterministic chaos [1,2]. Chaotic dripping was originally suggested by Rössler [2] and experimentally confirmed by Shaw and his collaborators [3]. Since then, many experimental and theoretical studies have established the dripping faucet as a sort of paradigm for chaotic systems [4–22]. Most previous studies have involved measuring the time interval T_n between successive drips, because the dripping

time is easily measured using a drop-counter apparatus [3–11]. The time intervals are then plotted in pairs (T_n, T_{n+1}) for each n to give a return map. Because the return maps typically appear low-dimensional, the behavior is often described by a simple dynamical model composed of a variable mass and a spring [3,7,12–16]. In this mass-spring model, a mass point, whose mass increases linearly with time at a given flow rate Q , oscillates with a fixed value of the spring constant k ; and a part Δm of the total mass m is removed when the spring extension exceeds a threshold, which describes the detachment of a falling drop. Although the model exhibits chaotic return maps similar to those obtained experimentally, its empirical nature means that it does not provide a unified explanation for the complex behavior of the real dripping faucets. Thus, the connec-

* Corresponding author.

E-mail address: k_kiyono@p.u-tokyo.ac.jp (K. Kiyono).

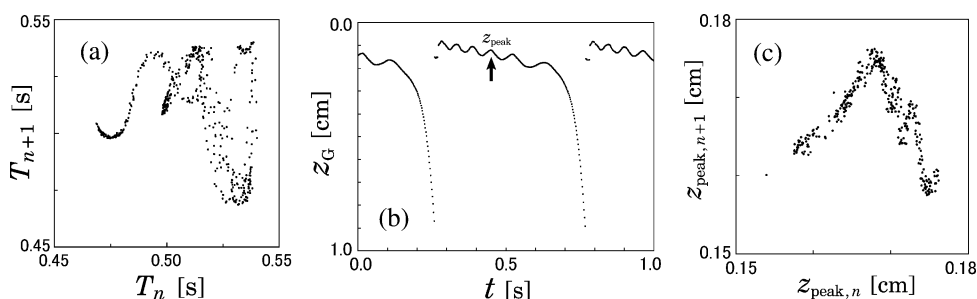


Fig. 1. Experiments on the dripping nozzle (7 mm inner diameter and 10 mm outer diameter). The flow rate $Q = 0.24$ g/s (~ 2 drips/s on average). (a) Return map of dripping time intervals, where the time intervals in pairs (T_n, T_{n+1}) for each n are plotted. The time series $\{T_n\}$ was measured using a drop-counter apparatus wherein a laser beam directed at a detector is interrupted whenever a falling drop crosses the beam. (b) Oscillation of the position z_G of the center of mass of the pendant drop under the nozzle. z_G was estimated from the shape of the pendant drop using the digitized image recorded by a high-speed video camera every 1/500 s. (c) Return map of the fourth peak $z_{peak,n}$ of the oscillating z_G , where $z_{peak,n}$ is indicated by an arrow in (b).

tion between the low-dimensional dynamical system and a presumably infinite-dimensional fluid dynamical system remains elusive.

Recently, we carried out fluid dynamic computations (FDC) based on a new algorithm involving Lagrangian description and succeeded in reproducing not only the time-dependent shapes of the pendant drops, but also various characteristics of chaotic dynamical systems [17]. A detailed analysis of our FDC made it possible to improve the mass-spring model by using more realistic approximations including taking into account the mass dependence of the spring constant, and the necking process [18]. This improved mass-spring model, described only by three variables: mass m , its position z_G and the velocity \dot{z}_G , closely described the dynamical behavior exhibited by the FDC. In particular, qualitatively good agreement among the bifurcation structure in parameter space (especially the repeating unit structure [18] which reflects the frequency of the oscillation of each pendant drop prior to its detachment), obtained by (i) the experiment [11], (ii) the FDC [17] and (iii) the improved mass-spring model [18], over a wide range of the control parameter Q provided a theoretical model of the basic low-dimensional structure inherent in the system, which is presented here.

An experimental chaotic attractor is shown in Fig. 1, which was a typical example of chaotic behavior observed at relatively low flow rates (for the nozzle diameter $5 \lesssim D \lesssim 10$ mm, $Q \lesssim 0.4$ g/s). As already been reported [11,18,22], the dripping spectra (the bifurcation diagrams vs. the flow rate Q) exhibit

that the range of period-one motion (in which the T_n value is unique) and that of non-period-one motion (T_n is not unique but distributed over a finite range) appear alternately and repeatedly as Q is increased. In the previous paper [17], we called this pattern “a unit structure”. A similar structure of the return map (Fig. 1(a)) was frequently observed in the different units, which suggests that the basic mechanism of chaotic dripping is the same in each unit. In addition to the discrete-time variable T_n , the mass $m(t)$ of the liquid suspended by the nozzle, the position of the center of mass $z_G(t)$ and velocity \dot{z}_G were also measured in our experiment. As seen in Fig. 1(b), $z_G(t)$ oscillates because the surface tension works as a restoring force. Similar oscillation was observed in both our FDC and improved mass-spring model [18]. Note that the frequency of the oscillation during each time interval T_n is determined by the flow rate. At $Q = 0.24$ g/s, z_G oscillates $6 \pm 1/2$ times before the breaking up and the phase of the oscillation in the plane (z_G, \dot{z}_G) fluctuates chaotically at breakup. A return map of $\{z_{peak,n}\}$ for every fourth peak of $z_G(t)$ is presented in Fig. 1(c). The return map of T_n (Fig. 1(a)) looks like an entangled string and thus the map function $T_{n+1} = G(T_n)$ cannot be single-valued. In contrast, the map function $z_{peak,n+1} = F(z_{peak,n})$ is approximately single-valued, although broadened by ‘noise’. Low-dimensional multi-valued map functions of T_n have often been obtained in both experiments [3–5,11], and numerical simulations [17,18]. For the improved mass-spring model [18], the map function $m_{r,n+1} = H(m_{r,n})$ ($m_{r,n}$ being the remnant mass just

after the n th breakup), as well as the map function $F(z_{\text{peak},n})$ is single-valued, while $G(T_n)$ is generally multi-valued. This is because the mapping of the time interval T_n is not topologically conjugate to that of the dynamical variable $m_{r,n}$. The FDC results also showed that $H(m_{r,n})$ is approximately single-valued even when $G(T_n)$ is multi-valued in a wide range of the flow rate [18]. Thus, T_n does not directly specify the state of the system despite its easy measurement.

Measurement of the continuous-time variables $\{z_G(t), \dot{z}_G(t), m(t)\}$ made it possible to visualize the reconstructed chaotic attractor in a continuous state space for the first time. The projection of the attractor in the plane (z_G, \dot{z}_G) corresponding to the chaotic motion in Fig. 1 is shown in Fig. 2 (top). On average, $z_G(t)$ oscillated six times during each time interval T_n (see Figs. 1(b) and 2 (top)). The cross sections of the attractor in insets of Fig. 2 look nearly one-dimensional and explicitly show that the motion of the pendant drop is well characterized by a few state variables. In a wide range of relatively small flow rate (for the nozzle diameter $5 \lesssim D \lesssim 10$ mm, $Q \lesssim 0.4$ g/s), approximately one-dimensional structure of cross sections was observed in both our experiment and FDC. The insets of Fig. 2 (top) show the existence of the stretching and folding mechanism, which plays an essential role in chaotic dynamics. The transition from the oscillating process to the ‘necking’ process occurs in the region S (Fig. 2) in which trajectories starting with slightly different remnant masses separate exponentially from each other. In the necking process a thin columnar bridge (between the pendant mass and the nascent drop) grows until the next breakup moment, as shown in Fig. 2(b). Immediately after the separation of the main drop the thin columnar bridge recoils as the tip is formed to a round knob and the secondary droplet (satellite drop) is pinched off within a time $\Delta t \sim 0.01$ s. The present analysis ignores the satellite drops. In Fig. 2 (bottom) the FDC results are presented including the return map of T_n (Fig. 2(a)) and profiles of a pendant drop prior to its detachment (Fig. 2(b)), which show qualitatively good agreement with the experimental observations. As will be shown in Fig. 3(b), the cross sections of the theoretical attractor also exhibit the low-dimensionality. An attractor in the space (z_G, \dot{z}_G, m) with a similar spiral structure has already been obtained using the improved mass-spring model [18]. These results strongly support the use of the three

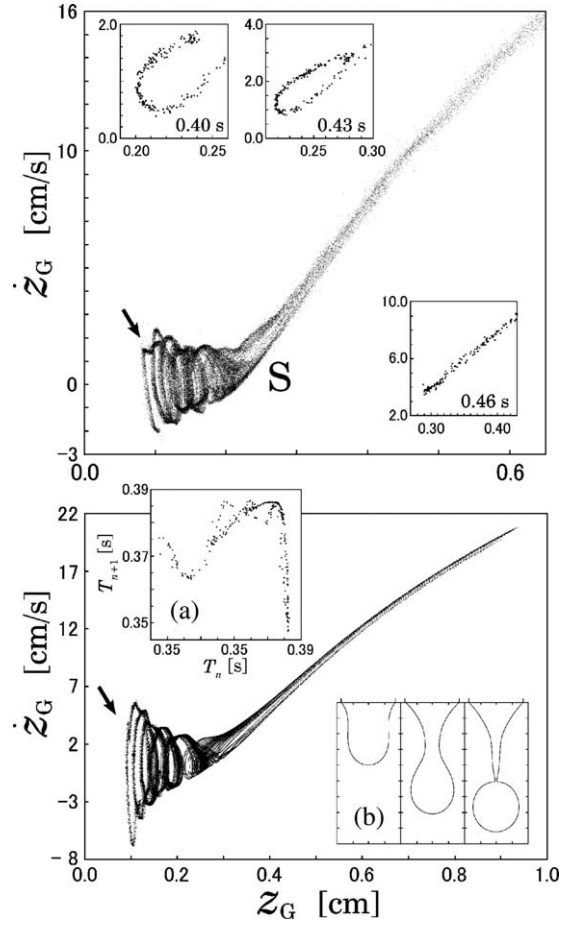


Fig. 2. The top panel is the experimentally observed strange attractor under the same experimental conditions as in Fig. 1, where the position z_G and the velocity \dot{z}_G of the pendant drop under the nozzle are plotted at every $1/500$ s. Insets are Poincaré cross sections of the attractor (plotting of \dot{z}_G vs. z_G) at time t measured from each breakup moment. The bottom panel is numerical simulations (FDC), where a dripping water faucet (7 mm diameter) is simulated at the flow rate $Q = 0.32$ g/s. We have used the same parameter values as in Ref. [18]. (a) Return map of dripping time intervals (cf. Fig. 1(a)); (b) profiles of a pendant drop prior to its detachment.

state variables: z_G , \dot{z}_G and m to describe the dripping faucet dynamics.

The motion of the pendant drop is subjected to gravitational force and surface tension. Since the surface energy depends on the shape of the pendant drop, the total potential energy U (i.e., gravitational plus surface) should be a function of the many degrees of freedom of the liquid. Our FDC show, however, that approximating U as a function of two variables,

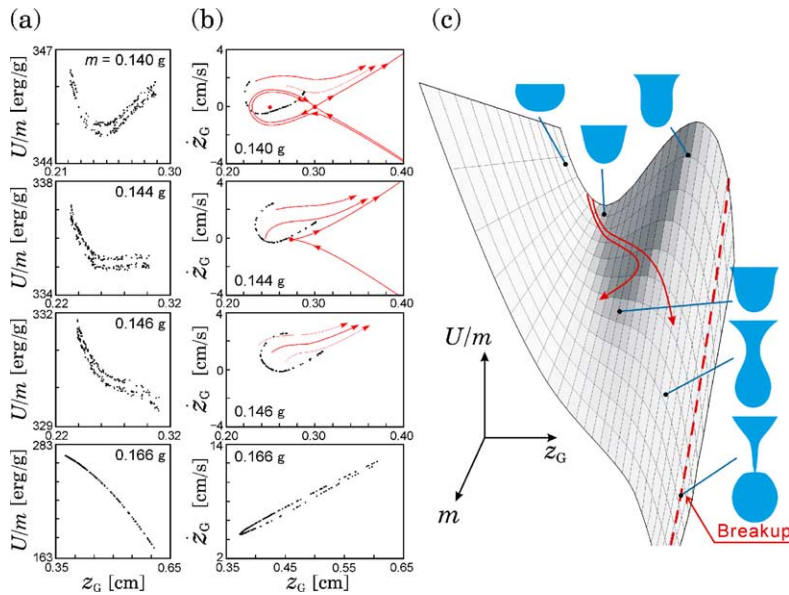


Fig. 3. (a) Fluid dynamic simulation (7 mm diameter, the flow rate $Q = 0.32$ g/s). Cross section of U/m for the attractor is plotted vs. z_G on a constant mass surface, where U/m is the total potential (= surface tension plus gravitation) energy per unit mass as a function of m (pendant drop mass in units of gram in each panel) and z_G (position of the center of mass). The critical mass $m_{\text{crit}} = 0.144$ g. (b) Black dots represent the Poincaré section of the attractor, plotting of \dot{z}_G vs. z_G , on the same constant mass surface as in (a) (obtained from the same simulation). The red solid curves indicate the flow in the state space, which were drawn by referring to the results obtained from another simulation with fixed mass (i.e., $Q = 0$). The red points in the top two panels are fixed points for the $Q = 0$ system. (c) Schematic view of a typical potential surface, obtained by approximating U/m in (a) by a single valued function of z_G and m . The pendant drop shapes (light blue) in various state points (z_G, m) on the potential surface are indicated. The red lines represent the trajectories starting with slightly different masses; one oscillates in the potential valley, while the other gets over the ridge because of a slight difference of the velocity \dot{z}_G . The breakup occurs on the red dashed line. For color see figure online.

m and z_G , yields a conceptually clear picture for the basic low-dimensional structure of the system. Cross sections of U/m , the potential energy per unit mass, at several fixed values of m for the chaotic attractor shown in Fig. 2 (bottom) are presented in Fig. 3(a). Poincaré cross sections at the same values of m as Fig. 3(a) are given in Fig. 3(b). Although the cross sections in Fig. 3(a) look two-folded, if they are approximated as single-valued functions, then a sheet of the potential surface $U(m, z_G)/m$ is obtained as shown in Fig. 3(c). The surface is characterized by a U-shaped valley and a ridge which converge as m increases and have totally merged when $m = m_{\text{crit}}$, the maximum mass of the static stable shape. We have also carried out a numerical experiment based on FDC with $Q = 0$ by fixing the value of m . Various artificial shapes of the pendant drops were used as initial conditions, and it was found that the point (m, z_G) rapidly converged onto

a well-defined potential surface $U(m, z_G)/m$ similar to that shown in Fig. 3(c). Besides the up and down-oscillation of the center of mass of the liquid, there are other oscillation modes which induce deformation of the pendant drop. These extra modes result in the fine structures of the attractor. For example, the map function in Fig. 1(c) shows two or three peaks apart from the main one. Close observation of the experimental and FDC results revealed that these fine structures correspond to the deformation modes of the liquid. A deformation mode can be seen in Fig. 2 as a sharp bend of the trajectory (arrows). This extra mode, which has not been previously observed, was found to be a collision of the pendant drop with the nozzle, triggered by the shock of breakup. The mode is rapidly decays and thus only affects the initial oscillation just after the break. Because of the excitation of the extra mode, the state point (m, z_G) separates from the well-defined surface $U(m, z_G)$ at the initial stage, and

rapidly returns (\sim ms) to the surface. This process stretches and folds the chaotic orbit, which makes the potential surface two-folded as in Fig. 3(a).

The potential surface for the closed system (i.e., the pendant drop for $Q = 0$) is useful for understanding the dynamics of the open system ($Q > 0$). A minimum and a maximum of $U(m, z_G)/m$ for the $Q = 0$ system correspond to a stable fixed point (static equilibrium shape) and a saddle point (unstable equilibrium shape, see Fig. 3(c)), respectively. These are indicated by red points in the top two panels of Fig. 3(b). When $m = m_{\text{crit}}$ ($= 0.144$ g), the stable fixed point disappears, and the necking process begins leading to the detachment of the drop. When $m < m_{\text{crit}}$, the trajectories of the pendant drops oscillate in the valley of $U(m, z_G)/m$, which corresponds to the spiral structure of the attractor in Fig. 2. The flow of the $Q = 0$ system as depicted in Fig. 3(b), also suggests that the state point of the pendant drop causes the spiral orbits in the phase space (z_G, \dot{z}_G, m) . The chaotic dynamics, especially the stretching and folding of the attractor, can be interpreted as follows. The stable fixed point approaches the saddle point as m increases. The state point thus visits the vicinity of the saddle point after the spiral motion, which causes the instability of the orbit, or equivalently, the stretching of the attractor. The Poincaré section of the chaotic attractor (Fig. 3(b)), which rotates around the stable fixed point with increasing m , is gradually crushed and asymptotes to a single line through the necking process.

The above analysis leads to the motion of the dripping faucet being described in terms of the approximate potential function U as

$$\ddot{z}_G = -\frac{\partial U(m, z_G)/m}{\partial z_G} - \frac{(\gamma + Q)}{m} \dot{z}_G, \quad \dot{m} = Q, \quad (1)$$

where γ is the damping constant. This equation describes the motion of a particle with unit mass in 2-dimensional space (m, z_G) , where the particle is forced to have a constant velocity $\dot{m} = Q$ in the direction of the m -axis. Our improved mass-spring model corresponds to a local quadratic approximation for the potential near the bottom $z_G = z_0$ of the valley in which the m -dependence of the spring constant $k(m) \equiv \partial^2 U(m, z_0)/\partial z_0^2$ has been included [18]. The present description is thus a natural extension of the improved mass-spring model. Results of the numeri-

cal simulations using Eq. (1) were in qualitative agreement with our experimental and FDC results. As we have seen, the picture of the global landscape of the potential is much clearer than the improved mass-spring model for intuitively understanding the dynamics of the system. If the flow rate Q is small enough so that the initial oscillation after the breakup is damped, the particle (equivalently the state point of the pendant drop) goes along the bottom of the valley as m increases. At $m = m_{\text{crit}}$, where the valley merges into the ridge, the particle's motion loses its stability (start of the necking process) and rapidly approaches the breakup point (on the broken red line in Fig. 3(c)). Since the instability always begins at the same point $m = m_{\text{crit}}$ in this case, the size of each falling drop is uniform. If, on the other hand, the oscillation of the pendant drop affects the start of necking, the dripping motion exhibits a variety of flow rate-dependent periodic and chaotic patterns. Note that the particle generally gets over the ridge before m reaches m_{crit} when it is oscillating. At a flow rate resulting in a chaotic motion, two trajectories starting with slightly different m values (different remnant masses) are initially close to each other. As m increases, however, one trajectory may get over the ridge at a certain m value, while the other remains in the valley owing to a small difference in \dot{z}_G (two red lines in Fig. 3(c)).

Similar potential landscapes are expected for other subjects involving drop formation like ink-jet printing [23] and atomization [24]. The potential surface describing the motion in the attractor was confirmed by FDC to have essentially the same topology even for high viscosity liquids and for microfluidic systems (drop size \sim pl). Hence, the present picture of a particle moving along a low-dimensional potential surface is relevant to modeling drop formation in general.

Acknowledgements

We are grateful to Professor W.S. Price and Professor A.L. Salas-Brito for careful reading of the manuscript. We also thank Professor Z.R. Struzik for helpful comments. This work was supported by grant from the Research Fellowships of the Japan Society for the Promotion of Science for Young Scientists.

References

- [1] J.P. Crutchfield, J.D. Farmer, N.H. Packard, R.S. Shaw, *Sci. Am.* 254 (12) (1986) 46;
E. Ott, *Chaos in Dynamical Systems*, Cambridge Univ. Press, New York, 1993;
J. Marston, *Nature* 379 (1996) 306.
- [2] O.E. Rössler, in: H. Haken (Ed.), *Synergetics: a Workshop: Proceedings of the International Workshop on Synergetics at Schloss Elmau, Bavaria*, Springer-Verlag, New York, 1977, p. 174.
- [3] R. Shaw, *The Dripping Faucet as a Model Chaotic System*, Aerial Press, Santa Cruz, 1984;
P. Martien, S.C. Pope, P.L. Scott, R.S. Shaw, *Phys. Lett. A* 110 (1985) 399.
- [4] H.N. Núñez-Yépez, A.L. Salas-Brito, C.A. Vargas, L. Vincente, *Eur. J. Phys.* 10 (1989) 99;
H.N. Núñez-Yépez, C. Carbajal, A.L. Salas-Brito, C.A. Vargas, L. Vincente, in: P. Cordero, B. Nachtergaele (Eds.), *Fluids, Solids and other Complex Systems*, Elsevier, Amsterdam, 1991, p. 467.
- [5] X. Wu, Z.A. Schelly, *Physica D* 40 (1989) 433.
- [6] R.F. Cahalan, H. Leidecher, G.D. Cahalan, *Comput. Phys.* 4 (1990) 368.
- [7] J. Austin, *Phys. Lett. A* 155 (1991) 148.
- [8] K. Dreyer, F.R. Hickey, *Am. J. Phys.* 59 (1991) 619.
- [9] J.C. Sartorelli, W.M. Gonçalves, R.D. Pinto, *Phys. Rev. E* 49 (1994) 3963.
- [10] T. Schmidt, M. Marhl, *Eur. J. Phys.* 18 (1997) 377.
- [11] T. Katsuyama, K. Nagata, *J. Phys. Soc. Jpn.* 68 (1999) 396.
- [12] G.I. Sánchez-Ortiz, A.L. Salas-Brito, *Physica D* 89 (1995) 151.
- [13] A. d'Innocenzo, L. Renna, *Phys. Rev. E* 58 (1998) 6847.
- [14] A. Ilaraza-Lomeli, C.M. Arizmendi, A.L. Salas-Brito, *Phys. Lett. A* 259 (1999) 115.
- [15] L. Renna, *Phys. Lett. A* 261 (1999) 162.
- [16] A.R. de Lima, T.J.P. Penna, P.M.C. de Oliveira, *Int. J. Mod. Phys. C* 8 (1997) 1073.
- [17] N. Fuchikami, S. Ishioka, K. Kiyono, *J. Phys. Soc. Jpn.* 68 (1999) 1185.
- [18] K. Kiyono, N. Fuchikami, *J. Phys. Soc. Jpn.* 68 (1999) 3259.
- [19] R.D. Pinto, J.C. Sartorelli, *Phys. Rev. E* 61 (2000) 342.
- [20] B. Ambravaneswaran, S.D. Phillips, O.A. Basaran, *Phys. Rev. Lett.* 85 (2000) 5332.
- [21] K. Kiyono, N. Fuchikami, *J. Phys. Soc. Jpn.* 71 (2002) 49.
- [22] A. D'Innocenzo, F. Paladini, L. Renna, *Phys. Rev. E* 65 (2002) 056208.
- [23] T.W. Shield, D.B. Bogy, F.E. Talke, *IBM J. Res. Dev.* 31 (1987) 96.
- [24] K. Amagai, M. Arai, in: *Proceedings of 3rd Conference ILASS-Asia*, 1998, p. 49.